Low Temperature Synthesis and Characterization of $Ni_xFe_{3-x}O_4$ (0≤x≤1.5) Electrodes for Oxygen Evolution Reaction in Alkaline Medium

Manish Kumar Yadav, Chinky Gangwar and Narendra Kumar Singh[*]

Department of Chemistry, Faculty of Science, University of Lucknow, Lucknow-226007 (INDIA)

Corresponding Author Email: [*]nksbhu@yahoo.com; singh_narendra@lkouniv.ac.in

ABSTRACT

Pure and nickel substituted spinel ferrites with composition $Ni_xFe_{3-x}O_4$ ($0 \le x \le 1.5$) have been synthesized to investigate their electrocatalytic properties for oxygen evolution reaction (OER) in alkaline medium by using co-precipitation method at 80 °C. Results of the pliminary examination (IR and XRD) specify the formation of almost pure spinel phase of the oxide. All the electrochemical charactrization such as cyclic voltammogram (CV), anodic polarization curve for the determination of electrocatalytic activity and thermodynamic parameters were done in three electrode single compartment glass cell. The study revels that nature of CV curve for each oxide electrode was same and exhibited a pair of redox peaks, one anodic (E_{Pa}= 509±22 mV) and a corresponding cathodic peak (E_{Pc}= 351±6 mV) prior to OER. The substitution of Ni in the Fe_3O_4 matrix increases the electrocatalytic activity and at E = 850 mV, it is ~7 times higher with $Ni_{1.5}Fe_{1.5}O_4$ (j = 158.0 mAcm^{-2}) than that of base oxide. For thermodynamic parameters, anodic polarization curve was recorded in 1M KOH at different temperatures. The standard electrochemical enthalpy of activation ($\Delta H_{el}^{\circ\neq}$) was found to be minimum with $Ni_{1.5}Fe_{1.5}O_4$. The standard enthalpy of activation ($\Delta H^{\circ\neq}$) and standard entropy of activation ($\Delta S^{\circ\neq}$) have also been calculated with the help of polarization curve recorded at different temperatures.

Keywords: Co-precipitation, nickel ferrites, SEM, XRD, electrocatalysis, activation energy

1. INTRODUCTION

Global expansion of urbanization and industrialization has increased the world's energy demand. Among available renewable and nonrenewable sources of energy, fossil fuels are directly or indirectly satisfying major portion of world's energy demand. However, in the race of maintaining sufficient supply of energy to every consumer, two big challenges has come to light, fossil fuel deposits are likely to remain adequate for next few generations [1] only and byproducts release from their combustion are creating adverse effect at our ecological system. In the search of non-conventional clean and efficient energy sources hydrogen has found to be very promising source with no harmful byproducts and it has also high energy density (140 MJ kg^{-1}). Apart from its application as a source of energy, hydrogen is also consumed in fertilizer production, food processing, metallurgical applications [2], therefore, global demand of hydrogen is growing approximately at the rate of 10% every year. However, again problem arises because 96% of hydrogen is produced from fossil fuels [2] which leave a carbon footprint. The clean way to produce hydrogen and oxygen of high purity is splitting of water through electrochemical route, but in this process large amount of energy loses due to the high value of oxygen overpotential for oxygen evolution reaction (OER) at anode and hydrogen overpotential for hydrogen evolution reaction (HER) at cathode. The application of efficient electrocatalyst is the key point to reduce overpotential because electrode process is dramatically affected by the electrode material [3]. In the last few decades various type of materials are being developed and used as electrocatalyst. In the series of development, various precious metals [4], metal alloys [5], bimelattic materials [6] metal oxides [7], metal mixed oxides of spinel [8, 9] and perovskite [10-13] type have been frequently used either in the form of coating at any base or itself as an electrode. In last two to three decades, spinel type mixed oxide are extensively explored not only because of their electrocatalytic properties but also these materials have versatile application in various fields because of their amazing physical and chemical properties. Spinel type oxides are used as catalyst in organic and inorganic reactions like acetylation of amines, alcohols and phenols [14], photodegradation of organic pollutant [15], oxidation of alkenes to aldehydes and epoxides [16], liquid phase Friedel-Craft alkylation [17], decomposition of hydrogen peroxide [18, 19], synthesis of ammonia [20], oxidation of butene to butadiene [21], as anode material in the synthesis of chlorine and chlorate [22] etc. Initially, these oxides were prepared by high temperature thermal decomposition [23] methods which requires prolong heating and materials obtained have low specific surface area as well as low electrocatalytic activity. During recent decades, various preparation methods like freeze-drying [24], citrate precursor techniques [25], co-precipitation [26], sol-gel [27], hydrothermal [28] etc. have been developed to obatain the spinel oxides. Out of these, the oxides prepared through sol-gel [29, 30] and co-precipitation [31, 32] are found to be more worthy, because of their low temperature operation and high degree of compositional control. Also, the prepared oxides possesses relatively better electrocatalytic activity and low overpotential. Recently Singh et al. [8, 9, 31, 33-39] used co-precipitation technique at controlled pH (= 11) for preparation of a series of binary and ternary ferrites by partially substituting iron atoms with different foreign metal ions in Fe_3O_4 matrix and found considerable enhancement in electrocatalytic activity towards OER. In the last few years, we [40-43] have also prepared cobalt, nickel and manganese

substituted ferrites and found improvement in activity towards OER in substituted oxides. The Ni-substituted spinel ferrites [40] were synthesized by novel egg-white sol-gel method as reported by Maensiri et al. [44]. In the synthesis, metal nitrates were taken in stoichiometric ratio and mixed in the solution of 60 ml freshly extracted egg-white (ovalbumin) and 40 ml of double distilled water. After stirring vigorously at 27 °C for 2 hrs, the homogeneous mixed solution was then evaporated in water bath at 80 °C until a dried precursor was obtained. The precursor was crushed into agate pestle mortar to get powder and then heat treated at 550 °C for 3 hrs to get the desired oxides. The electrode of the oxide was prepared on Ni-support for all the electrochemical characterization. Tao et al. [45] has synthesized the copper substituted ferrite material by adopting co-precipitation method at very low temperature and analyzed their gas sensing properties. By adopting the same preparation method, we prepared pure and nickel substituted ferrite materials and studied their physicochemical and electrochemical properties towards OER in alkaline medium. In particular, the originality of this work consists of drying the material at room temperature, crushed in agate pastel mortar and heated overnight at 80°C in a muffle furnace (ASCO) to get the desired oxide. The results obtained in the present study are described in this paper.

2. EXPERIMENTAL

2.1 Materials (Mixed Oxide Catalyst) Synthesis

Spinel-type mixed oxides having general formula $Ni_xFe_{3-x}O_4$ (x=0, 0.5, 1.0 and 1.5) were prepared by using low temperature coprecipitaion method [45]. In the process of preparation, analytical grade (Merck) metal nitrates of iron and nickel [$Fe(NO_3).9H_2O$ & $Ni(NO_3).6H_2O$] were used as metal ion source and a aqueous 4M sodium hydroxide solution was used for precipitation. In the typical process, statichiometric amount of metal nitrates were weighed and dissolved in 100 ml double distilled water at room temperature and 75 ml hot solution of 4M NaOH was added slowly to get the precipitates of metal hydroxides. The obtained precipitate was kept in water bath at 90°C for 2 hours and it was then filtered and washed several times with redistilled water to avoid the presence of sodium ion in it. Further, The material was dried at room temperature, crushed in agate pastel mortar and heated overnight at 80°C in a muffle furnace (ASCO) to get the desired oxide.

2.2 Characterization of Oxides

Morphology of the sintered oxides was analyzed with a scanning electron microscope (SEM, LEO 430). To confirm the spinel ferrite phase, IR spectra was recorded in the wavenumber region 4000–400 cm^{-1} by using FTIR Thermoscientific (Nicole-6700) spectrometer. For the purpose, oxide powder was mixed with purified potassium bromide in an agate pastel mortar and then transferred into pellet by using pelletizer at 5 ton. The powder X-ray diffractometer (XPERT-PRO diffractometer, Model: PW 3050/60) composed with Cu-K_α as radition source (λ=1.54048 Å) was used to record the X-ray diffraction (XRD) pattern and determine the phase and crystallite size of the material.

2.3 Fabrication of Film Electrode

The materials, so obtained, were converted into film electrode on a pre-treated nickel plate by using oxide slurry painting technique. In this technique, a small amount of powdered oxide was mixed with few drops of triton X-100 in an agate pastel mortar and made a pasty mass (slurry). It was then applied over the one side of pre-treated nickel (Aldrich 99.9%) plate with the help of fine brush and subsequently heat treated at 380°C for 1.5 hr in an electrical muffle furnace to get the adherent oxide film. If required, the process was repeated two or three times to get the desired loading of oxide over the metal plate. Prior to paint the oxide slurry, the nickel substrate (~1.5 cm^2 area) was polished mechanically with a fine emery paper, followed by treatment with concentrate hydrochloric acid for about 20 minutes, washed with distilled water, degreased in acetone and finally washed with redistilled water and air dried. To achieve the better adherence of oxide film over the metal plate, the plate was removed only when the furnace was attended the temperature < 80°C. In order to use the coated nickel plate as electrode, a commercial grade plastic coated copper wire (1 mm thick, 15 cm length) is connected at uncoated side of nickel plate as describe in literature [46]. Only a small oxide coated area (~ 0.5 cm^2) was used for all types of electrochemical analysis of oxide material and remaining portion of both surfaces of the nickel plate was coated with a non-conducting layer of araldite epoxy adhesive.

2.4 Electrochemical Instrument and Cell Setup

A conventional three electrode single compartment glass cell attached with a Potentiostat/Galvanostat (Gamry Reference 600ZRA) was used for all types of electrochemical analyses. The instrument is associated with a personal computer having corrosion and physical electrochemistry software. Hg/HgO/1M KOH (E°=0.098 V vs. NHE at 25°C) was used as reference electrode and a platinum foil of approximately ~2 cm^2 area as counter electrode. The counter and working (oxide film) electrodes were inserted directly in the solution compartment, while the reference electrode was connected with cell solution through a luggin capillary (KCl/Agar-Agar salt bridge). It was done to minimize the solution resistance (iR drop) between working and reference electrodes.

3. RESULTS AND DISCUSSION

3.1 Scanning Electron Micrograph (SEM)

Surface morphology of sintered oxide materials was determined by recording scanning electron micrograph at the magnification of 2500 X. Images, so obtained, are shown in the Figure 1. It reveals that the grain size are not much affected by the substitution of Ni in base oxide. However, among all oxides the texture of the $NiFe_2O_4$ is seemed to be more homogeneous and porous with minimum grain size.

3.2 Infrared Study (IR)

Figure 2 represents the IR spectra of the oxides recorded in the wavenumber refion 4000-400 cm^{-1}. Spectra exhebited two characteristic absorption bands of spinel ferrite ν_1 at 598-566 cm^{-1} and ν_2 at 496-455 cm^{-1} [47, 48] and correspond to tetrahedral and octahedral sublattice sites, respectively. The observed broad band at ~ 3430 cm^{-1} and less intense peak at ~1628 cm^{-1} resemble to the O-H stretching vibrations.
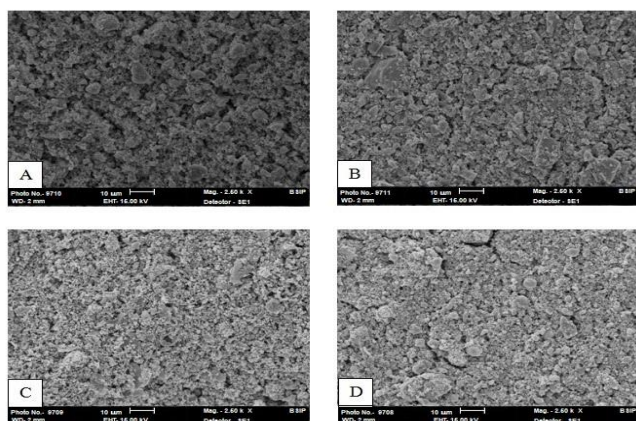

Figure 1. SE Micrographs of oxide powder sintered at 80°C for 12 h at magnification (2500 X). A: Fe_3O_4; B: $Ni_{0.5}Fe_{2.5}O_4$; C: $NiFe_2O_4$; D: $Ni_{1.5}Fe_{1.5}O_4$
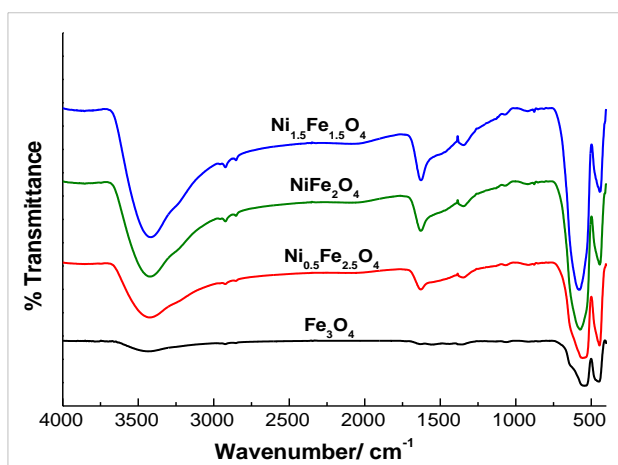

Figure 2. IR Spectra of $Ni_xFe_{3-x}O_4$ (0 ≤ x ≤ 1.5) oxides sintered at 80°C for 12 h

3.3 Powder X-Ray Diffraction (XRD)

The XRD pattern of sintered oxides was recorded in the 2θ range 20° to 70° and shown in Figure 3. The values of 2θ and corresponding miller indices (hkl) are observed to be best coordinate with JCPDS ASTM file 44-1485 for $NiFe_2O_4$. The peaks corresponding to the planes (220), (311), (400), (422), (511) and (400) confirms the formation of cubic spinel structure. The most intense diffraction pattern (311) of each oxide was used to calculate the crystallite size by applying Debye-Scherer's formula [49]. The calculated values are 46, 35, 24 and 31 nm for Fe_3O_4, $Ni_{0.5}Fe_{2.5}O_4$, $NiFe_2O_4$ and $Ni_{1.5}Fe_{1.5}O_4$, respectively.

3.4 Cyclic Voltammetry (CV)

To know the redox behavior of surface electroactive species with regards to oxidation-reduction reaction, cyclic voltammogram of each oxide film electrode was recorded in 1M KOH at 25°C. Each Voltammogram was recorded between the potential window 0.0-0.7 V at the scan rate (SR) of 20 mV sec^{-1} and shown in Fig. 4. From figure, it reveals that each CV curve exhibited an anodic peak (E_{Pa}= 509±22 mV) and a corresponding cathodic peak (E_{Pc}= 351±6 mV) prior to the onset of oxygen evolution reaction regardless of nature of oxide film.
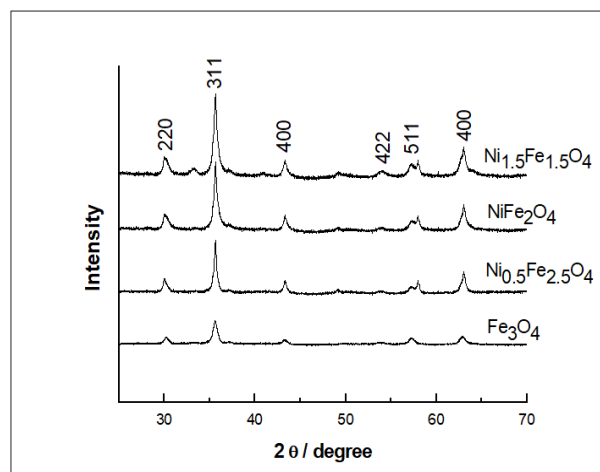

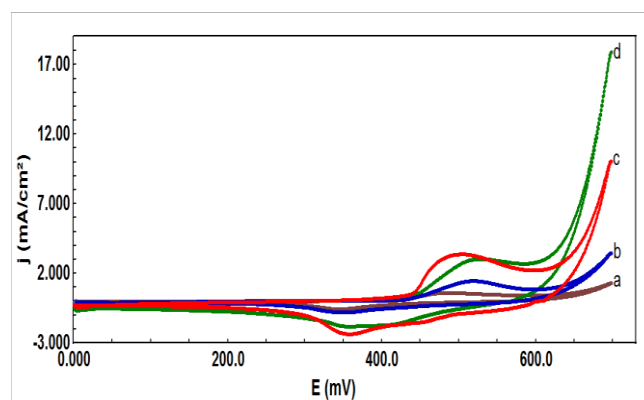**Figure 3.** XRD powder patterns of $Ni_xFe_{3-x}O_4$ (0 ≤ x ≤ 1.5), sintered at 80ºC for 12 h

Figure 4. Cyclic voltammogram of $Ni/Ni_xFe_{3-x}O_4$ (0 ≤ x ≤ 1.5) electrode in 1M KOH (SR = 20 mV/sec), a: Fe_3O_4, b: $Ni_{0.5}Fe_{2.5}O_4$, c: $Ni_{1.5}Fe_{1.5}O_4$, d: $NiFe_2O_4$

The peak potential (E_{Pa} & E_{Pc}), peak separation potential ($\Delta E_p = E_{Pa}-E_{Pc}$), formal redox potential [$E°=(E_{Pa} + E_{Pc})/2$], anodic (j_{P_a}) & cathodic (j_{P_c}) peak current and voltametric charge (q) were estimated from the CV curve and are listed in Table 1. The values of redox peak potentials ($E_{pa} \approx 490$ mV & $E_{pc} \approx 380$ mV) for bare Nickel electrode in 1M KOH at 298 K vs. Hg/HgO/KOH(1M) (E°=0.098V vs. NHE) [50] shows that the anodic and cathodic peaks found in case of prepared oxide film electrodes are due to transition of Ni(II)/Ni(III) redox couple [31]. It is also known that the oxides synthesized at low temperature are hygroscopic [31] in nature and does not protect the nickel substrate well from the electrolyte contact. However, this does not affect the stability of catalytic over

layer. The electrolyte might reach to substrate (Ni support) through pores, cracks, intercrystalline gaps formed in the catalytic film.

CV curves were also recorded at varying scan rates from 20-120 mV sec⁻¹ under similar experimental conditions. The representative voltammograms for $Ni/Ni_{0.5}Fe_{2.5}O_4$ is shown in Figure 5. The nature of the curve is similar to that recorded at 20 mV sec⁻¹ scan rate and exhibited a pair of redox peaks. However, shifting of anodic and cathodic peak potential is observed with the increase of SR from 20 to 120 mVsec⁻¹. The shift was found to be 31-93 mV and 12-25 mV in anodic and cathodic peak potentials, respectively. The anodic (j_{P_a}) and cathodic (j_{P_c}) peak current density value also increases linearly with increase in scan rate. At SR 20 mVsec⁻¹, the ratio of anodic and cathodic peak current density (j_{P_a}/j_{P_c}) are more than unity except Fe_3O_4. This indicates the irreversible nature [51-53] of the redox couple. The voltammetric charge (q) was estimated by integrating the CV curve from zero to a potential just prior to the start point of oxygen evolution [54]. The plot of voltammetric charge (q) vs. (scan rate)⁻¹/² was constructed for each oxide catalyst and shown in the Fig. 6. The linearity in the nature of the plot indicates that the surface redox process is diffusion controlled [54].

Table 1. Values of the Cyclic Voltammetric parameters of $Ni/Ni_xFe_{3-x}O_4$ ($0 \leq X \leq 1.5$) in 1 M KOH at 25°C (SR=20 mV sec⁻¹).

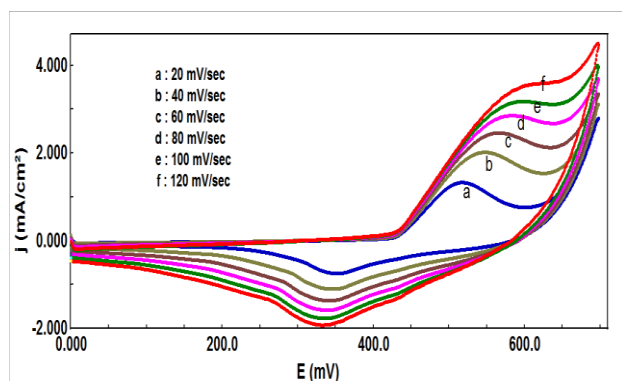| Electrode	E_{P_a} /mV	E_{P_c} /mV	ΔE_P /mV	E^o /mV	j_{P_a} /mA cm⁻²	j_{P_c} /mA cm⁻²	$\dfrac{j_{P_a}}{j_{P_c}}$	q /mC cm⁻²
Fe_3O_4	487	345	142	416	0.6	0.6	1.0	8.4
$Ni_{0.5}Fe_{2.5}O_4$	518	352	166	435	1.3	0.7	1.8	15.2
$NiFe_2O_4$	530	358	172	444	3.0	1.8	1.7	37.7
$Ni_{1.5}Fe_{1.5}O_4$	504	358	146	431	3.4	2.4	1.4	47.7

Figure 5. Cyclic voltammogram of the $Ni/Ni_{0.5}Fe_{2.5}O_4$ film electrode at different SR in 1M KOH (25°C).
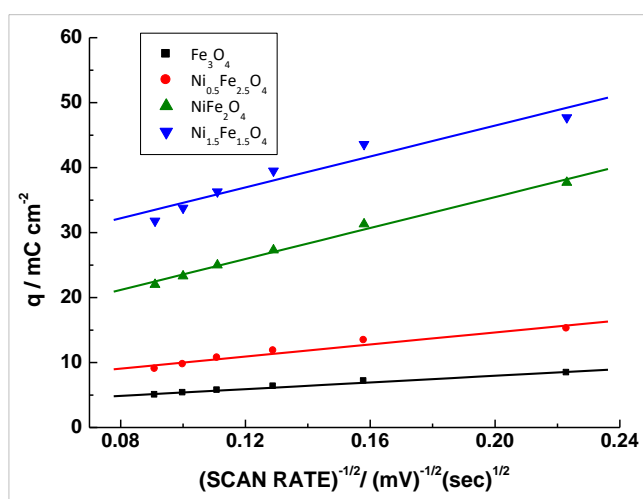

Figure 6. Plot of voltammetric charge (q) vs (scan rate)⁻¹/² for $Ni_xFe_{3-x}O_4$ ($0 \leq x \leq 1.5$) films on Ni in 1M KOH (25°C).

3.5 Electrocatalytic Activity

iR-compensated anodic Tafel polarization curve (log j vs. E) was recorded at slow SR (0.2 mV sec⁻¹) to determine the electrocatalytic activity of the oxide film electrode towards oxygen evolution reaction (OER). The polarization curve recorded in 1M KOH at 25°C for each oxide catalyst is shown in Figure 7. Values of electrode kinetic parameters estimated from the polarization curve is listed in Table 2. The nature of curves is almost same in low potential region. However in higher potential region some oxide electrocatalysts ($Ni_{0.5}Fe_{2.5}O_4$ and $NiFe_2O_4$) get more polarized than others and as a result of this the sequence of electrocatalytic activity of nickel substituted catalysts is found different in lower and higher potential regions. In lower potential regions (at 750 mV), the 1.0 mol Ni-substituted (45.1 mA cm⁻²) oxide was observed to be more active than 1.5 mol Ni-substituted (28.0 mA cm⁻²) oxide. But, in higher potential region (at 850 mV), the activity of both oxides is found in reverse order (158.0 mA cm⁻² for $Ni_{1.5}Fe_{1.5}O_4$ and 107.0 mA cm⁻² for $NiFe_2O_4$). Overall, the substitition Ni for Fe in the Fe_3O_4 mattrix enhanced the electrocatalytic activity and in terms of current density at a fixed potntial (E = 850 mV), activity of oxides followed the order;

$Ni_{1.5}Fe_{1.5}O_4$ (j=158.0 mA cm⁻²)>$NiFe_2O_4$ (j=107.0 mA cm⁻²)>$Ni_{0.5}Fe_{2.5}O_4$ (j=89.4 mA cm⁻²)>Fe_3O_4 (j=23.7 mA cm⁻²)
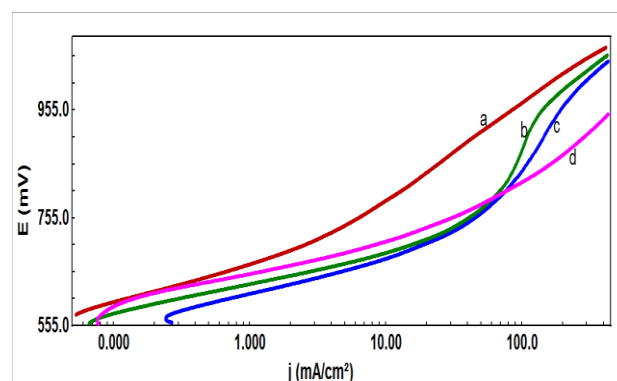

Figure 7. Tafel plots for the pure and Ni-substituted ferrite film electrodes on Ni in 1M KOH (25°C); SR: 0.2 mVsec⁻¹, a: Fe_3O_4, b: $Ni_{0.5}Fe_{2.5}O_4$, c: $NiFe_2O_4$, d: $Ni_{1.5}Fe_{1.5}O_4$.

Tafel slope (b) value was observed to decrease with the Ni-substitution and ranged between 50-68 mV decade⁻¹. The raction order (p) for OER with respect to hydroxide ion

concentration was determined by recording anodic Tafel polarization curves at varying KOH concentrations. In order to keep the electrical intensity uniform, the ionic strength of the electrolytic solution was maintained constant (μ=1.5) by adding an inert electrolyte KNO_3. A set of polarization curves for $Ni_{0.5}Fe_{2.5}O_4$ film electrode is shown in Figure 8. Values of current density were determined from the polarization curves at different potentials (625-700 mV) in the first Tafel region. A plot of log j vs. log [OH] was constructed and shown in Fig. 9. The order of reaction was estiated by measuring the slope of straight line. Figure 9 shows that at each potential the value of reaction order is same. Therefore, potential does not affect the value of reaction order when determined in the same Tafel region. Similarly, the order of reaction for each oxide electrocatalyst was determined by constructing the log j vs. log [OH] plot (Figure 10 and Table 2) at a fixed potential (E = 650 mV). A fractional order of reaction is obtained except $Ni_{1.5}Fe_{1.5}O_4$ electrode. Values of Tafel slope and reaction order indicate that the oxide electrodes follow different mechanistic path.

The electrocatalytic activity of the oxide electrode, $Ni_{1.5}Fe_{1.5}O_4$, of the present study is campared with spinel oxides obtained by other methods. At current density (j = 100 $mAcm^{-2}$), the oxide produced lower potential value over most

of the oxides. For instance, Iwakura et al. [23] observed 883 mV for $MnFe_2O_4$ in 1M KOH at 25°C at relatively low current density of 10 $mAcm^{-2}$. Orehotsky et al. [24] observed similar current density at E = 643 mV in 30 wt% KOH. Al-Mayouf et al. [55] found (j=18.7 $mAcm^{-2}$ at E=750 mV) for $Co_{0.5}Fe_{2.5}O_4$ prepared by hydrothermal method. Further, the oxide is much more active than obtained by NH_4OH sol-gel auto combustion [42] (j=100 $mAcm^{-2}$ at E=828 mV), NH_4OH COP [56] (j=100 $mAcm^{-2}$ at E=886 mV), egg-white sol-gel [40] (j=100 $mAcm^{-2}$ at E=865 mV) methods, which are recently reported in literature.

It is noteworthy that oxides in the present study and similar oxides prepared by egg-white sol-gel [40] route, both have almost same crystallite size. However, a significant variances have been observed in the morphological study. In the present study, oxides appears to be distribuited homogeneously with some small porosity. In contrary, the oxides obtained by egg-white sol-gel method [40] have some agglomaration. But, some cavity has been observed in the texture of the oxide in this work. Since texture plays a vital role in the electrocatalytic properties of the material, the higher electrocatalytic activity of the oxides obtained in the present study might be due to the superior morphological structure.

Table 2. Electrode kinetic parameters for oxygen evolution reaction on $Ni/Ni_xFe_{3-x}O_4$ (0≤x≤1.5) electrodes in 1 M KOH at 25°C.

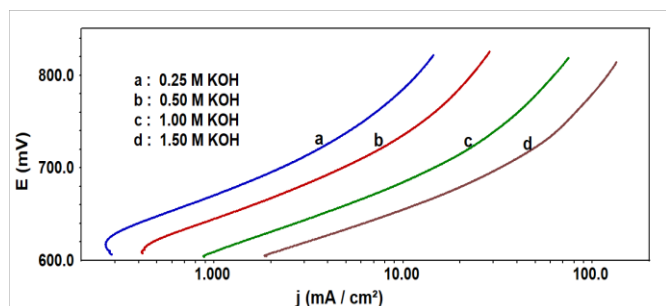| Electrode	Tafel slope /mVd^{-1}	Order (p)	E/mV at j ($mA\ cm^{-2}$)		j ($mA\ cm^{-2}$) at E/mV	
			10	100	750	850
Fe_3O_4	68	1.3	787	965	5.9	23.7
$Ni_{0.5}Fe_{2.5}O_4$	55	1.6	692	883	37.6	89.4
$NiFe_2O_4$	56	1.5	674	841	45.1	107.0
$Ni_{1.5}Fe_{1.5}O_4$	50	1.0	708	819	28.0	158.0

Figure 8. Tafel plots for the $Ni_{0.5}Fe_{2.5}O_4$ film electrode on Ni at varying KOH concentrations (μ=1.5) at 25°C

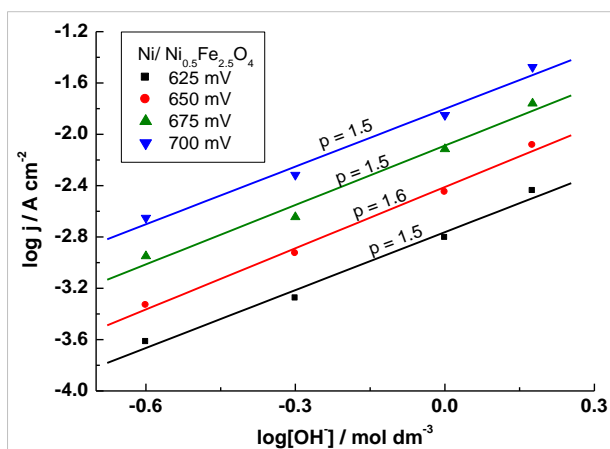**Figure 9.** Plot of log j vs log [OH] at a different applied potential for $Ni_{0.5}Fe_{2.5}O_4$ film electrode on Ni at 25°C

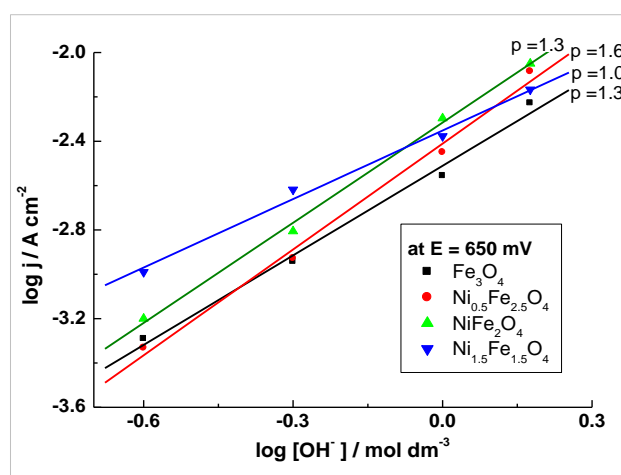**Figure 10.** Plot of log j vs log [OH] at a constant applied potential for $Ni/Ni_xFe_{3-x}O_4$ (0≤x≤1.5) film electrodes at 25°C

3.6 Thermodynamic Parameters

The influence of temperature at OER has also been studied on each oxide catalyst in 1M KOH. For the purpose, anodic Tafel polarization curves were recorded at varying temperatures, 20, 30, 40 and 50°C. A set of representative curve for the case of $Ni_{1.5}Fe_{1.5}O_4$ is shown in Figure 11. It is noted that during experiment, the temperature of working electrode was varied however, reference electrode was kept at constant temperature (at 25°C). Values of current density (log j) from the first linear region of the polarization curve were

estimated at constant potential (E=650 mV) and then plotted against 1/T (Figure 12). Values of standard electrochemical enthalpy of activation ($\Delta H_{el}^{o\neq}$) was calculated from the slope of the Arrhenius plot and found to be in the range between 45.4 - 67.7 kJ mol^{-1} with minimum value for most active, $Ni_{1.5}Fe_{1.5}O_4$ electrode.
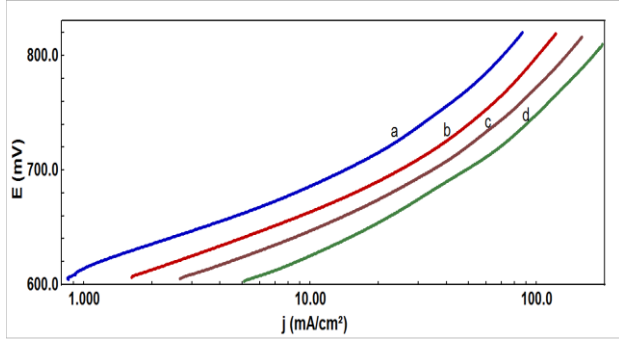

Figure 11. Tafel plots for the $Ni_{1.5}Fe_{1.5}O_4$ film electrode on Ni at different temperatures in 1 M KOH. a: 20°C; b: 30°C; c: 40°C; d: 50°C
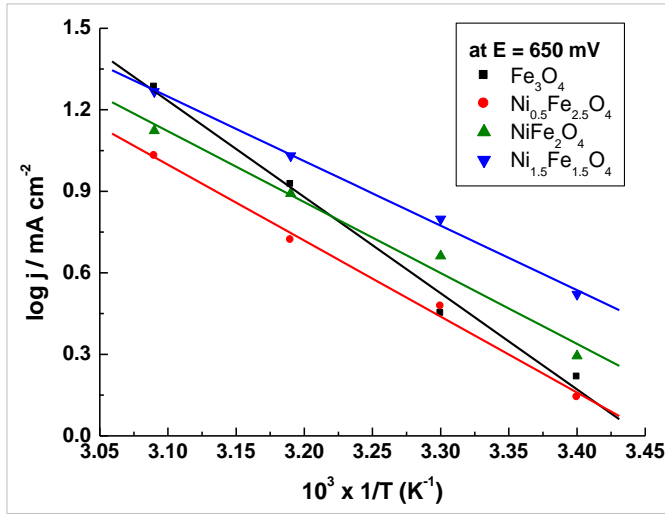

Figure 12. The Arrhenius plot at a constant applied potential for $Ni/Ni_xFe_{3-x}O_4$ (0≤x≤1.5) in 1 M KOH

Other thermodynamic parameters such as, standard enthalpy of activation ($\Delta H^{o\neq}$) and Standard entropy of activation ($\Delta S^{o\neq}$) were calculated by using the relations (1) and (2), respectively. [57];

$$\Delta H_{el}^{o\neq} = \Delta H^{o\neq} - \alpha F\eta \qquad (1)$$

where, α (=2.303RT/bF) is the transfer coefficient. η is the overpotential equal to E - E_{O2/OH^-}, where E is the potential applied and E_{O2/OH^-} (=0.303 V vs. Hg/HgO) [58] is the theoretical equilibrium Nernst potential in 1 M KOH at 25 °C. The value of 'b' is determined from the polarization curve obtained at different temperatures. R, F are the universal constants and T is the absolute temperature.

$$\Delta S^{o\neq} = 2.3R \left[\log j + \frac{\Delta H_{el}^{o\neq}}{2.3RT} - \log (nF\omega C_{OH^-}) \right] \qquad (2)$$

Here, ω is the frequency term and equal to $k_B T/h$. k_B and h are the Boltzmann and Plank's constant, respectively. In this

case, the value of n is taken 2. The estimated values of thermodynamic parameters are listed in the Table 3.

The relation (1) indicates that the value of $\Delta H_{el}^{o\neq}$ is reduced as the applied potential is increased. Similar trend has also been observed when Arrhenius plots (i.e. log j vs. 1/T) is constructed for $NiFe_2O_4$ (Figure 13) electrode at different potentials ranging from 625 to 700 mV. It is noteworthy that the values of $\Delta H_{el}^{o\neq}$ for each Ni substituted film electrodes are lower than that found on $Co_{1.5}Fe_{1.5}O_4$ (67.9 kJ mol^{-1}) [42] and almost similar for Adams-RuO$_2$ ($\Delta H_{el}^{o\neq}$ =49 kJ mol^{-1}) [59], $Co_{50}Ni_{25}B_{10}$ alloy ($\Delta H_{el}^{o\neq}$ =40 kJ mol^{-1} with) [60] and $Cu_{0.9}Co_{2.1}O_4$ ($\Delta H_{el}^{o\neq}$ =45 kJ mol^{-1}) [61], while higher than $Ni_{0.5}Fe_{2.5}O_4$ (38.4 kJ mol^{-1}), $NiFe_2O_4$ (42.7 kJ mol^{-1}) reported by us [40]. The highly negative value of $\Delta S^{o\neq}$ indicates the presence of adsorption phenomenon in the electrochemical formation of oxygen.
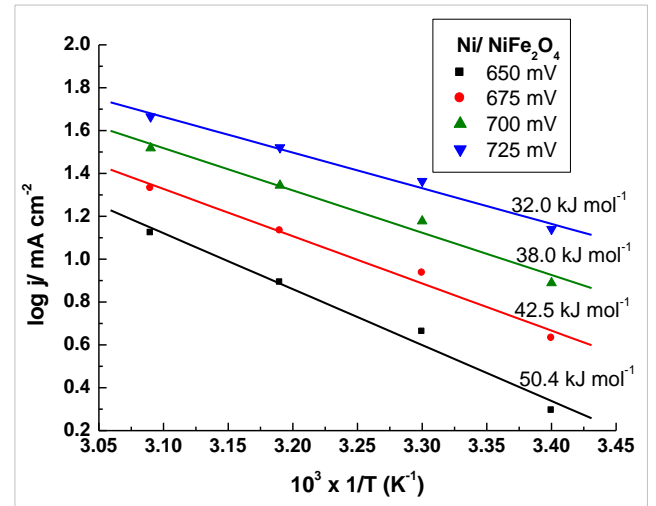

Figure 13. The Arrhenius plot at different applied potentials for $NiFe_2O_4$ on Ni in 1 M KOH

Table 3. Thermodynamic parameters for O_2 evolution on Ni / $Ni_xFe_{3-x}O_4$ (0≤x≤1.5) in 1 M KOH

Electrode	$\Delta H_{el}^{o\neq}$ (kJ mol^{-1}) at E = 650 mV	- $\Delta S^{o\neq}$ (J deg^{-1} mol^{-1})	α	$\Delta H^{o\neq}$ (kJ mol^{-1})
Fe_3O_4	67.7	122.7	0.8	96.8
$Ni_{0.5}Fe_{2.5}O_4$	53.5	159.6	1.0	89..3
$NiFe_2O_4$	49.9	166.1	1.0	85.1
$Ni_{1.5}Fe_{1.5}O_4$	45.4	192.1	1.1	82.2

4. CONCLUSION

The IR and powder XRD study showed the formation of spinel phase in prepared ferrite materials. Substitution of nickel in Fe_3O_4-matrix enhanced the electrocatalytic activity towards oxygen evolution reaction. At lower potential side the oxide, $NiFe_2O_4$, has highest electrocatalytic activity. However, due to polarization its activity reduced at higher potential value. Based on current density at 850 mV, 1.0 mol Ni substituted oxide (j= 158.0 mA cm^{-2}) was found most active, which is ~7 times higher than the base oxide. The higher electrocatalytic activity of the oxides obtained in the present study might be due to the existence of cavities in their texture. Those cavities might be responsable of their superior morphological structure which sustains high electrocatalytic activity for the OER.

ACKNOWLEDGMENT

REFERENCES

[1] Dresselhaus, M.S., Thomas, I.L. (2001). Alternative energy technologies. Nature, 414(6861): 332-337. https://doi.org/10. 1038/35104599

[2] Naterer, G.F., Fowler, M., Cotton, J., Gabriel, K. (2008). Synergistic roles of off-peak electrolysis and thermochemical production of hydrogen from nuclear energy in Canada. Hydrogen Energy, 33(23): 6849-6857. https://doi.org/10.1016/j.ijhydene.2008.09.011

[3] Trasatti, S. (2000). Electrocatalysis: understanding the success of DSA. Electrochim Acta, 45(15-16): 2377-2385. https://doi.org/10.1016/S0013-4686(00)00338-8

[4] Bockris, J.O.M., Srinivasan, S. (1969). Fuel Cells: Their Electrochemistry, McGraw-Hills, New York.

[5] Sasaki, K., Wang, J.X., Balasubramanian, M., McBreen, J., Uribe, F., Adzic, R.R. (2004). Ultra-low platinum content fuel cell anode electrocatalyst with a long-term performance stability. Electrochim Acta, 49(22-23): 3873-3877.
https://doi.org/10.1016/j.electacta.2004.01.086

[6] Lima, F.H.B., Sanches, C.D., Ticianelli, E.A. (2005). Physical Characterization and Electrochemical Activity of Bimetallic Platinum-Silver Particles for Oxygen Reduction in Alkaline Electrolyte. Electrochem. Soc., 152(7): A1466-A1473.
https://doi.org/10.1149/1.1933514

[7] Trasatti, S. (1991). Physical electrochemistry of ceramic oxides. Electrochim Acta, 36(2): 225-241. https://doi.org/10.1016/0013-4686(91)85244-2

[8] Singh, R.N., Singh, N.K., Singh, J.P. (2002). Electrocatalytic properties of new active ternary ferrite film anodes for O$_2$ evolution in alkaline medium. Electrochim. Acta, 47(24): 3873-3879. https://doi.org/10.1016/ S0013-4686(02)00354-7

[9] Singh, R.N., Singh, N.K., Singh, J.P., Balaji, G., Gajbhye, N.S. (2006). Effect of partial substitution of Cr on the electrocatalytic properties of CoFe$_2$O$_4$ towards O$_2$-evolution in alkaline medium. Hydrogen Energy, 31(6): 701-707. https://doi.org/10.1016/j.ijhydene.2005.07.0 03

[10] Singh, N.K., Tiwari, S.K., Singh, R.N. (1998). Electrocatalytic properties of lanthanum manganites obtained by a novel malic acid-aided route. hydrogen Energy, 23(9): 775-780. https://doi.org/10.1016/S03603199 (97)00119-5

[11] Sharma, T., Singh, N.K., Tiwari, S.K., Singh, R.N. (1998). Electrocatalytic properties of La-manganites prepared by low temperature synthesis. Eng. Mat. Sci., 5: 38-42. http://hdl.handle.net/123456789/29573

[12] Singh, N.K., Lal, B., Singh, R.N. (2002). Electrocatalytic properties of perovskite-type La$_{1-x}$Sr$_x$MnO$_3$ obtained by a novel sol–gel route for O$_2$ evolution in KOH solutions.

hydrogen Energy, 27(9): 885-893. https://doi.org/10.1016 /S0360-3199(02)00008-3

[13] Singh, N.K., Yadav, M.K., Fernandez, C. (2017). Electrocatalytic properties of La1-xCuxCoO$_3$ (0≤ X≤ 0.8) film electrodes prepared by Malic Acid sol-gel method at pH=3.75. Electrochem. Sci., 12(8): 7128-7141. https://doi.org/10.20964/2017.08.68

[14] Farhadi, S., Panahandehjoo, S. (2010). Spinel-type zinc aluminate (ZnAl2O4) nanoparticles prepared by the co-precipitation method: A novel, green and recyclable heterogeneous catalyst for the acetylation of amines, alcohols and phenols under solvent-free conditions. Applied Catalysis A: General, 382(2): 293-302. https://doi.org/10.1016/j.apcata.2010.05.005

[15] Anchieta, C.G., Sallet, D., Foletto, E.L., da Silva, S.S., Chiavone-Filho, O., do Nascimento, C.A.O. (2014). Synthesis of ternary zinc spinel oxides and their application in the photodegradation of organic pollutant, Ceramics Int., 40(3): 4173-4178. https://doi.org/10.1016/j.cer amint.2013.08.074

[16] Kooti, M., Afshari, M. (2012). Magnetic cobalt ferrite nanoparticles as an efficient catalyst for oxidation of alkenes, Scientia Iranica, 19(6): 1991-1995. https://doi.org /10.1016/j.scient.2012.05.005

[17] Ghorpande, S.P., Darshane, V.S., Dixit, S.G. (1998). Liquid-phase Friedel-Crafts alkylation using CuCr$_{2-x}$Fe$_x$O$_4$ spinel catalysts, Applied Catalysis A: General, 166(1): 135-142. https://doi.org/10.1016/S0 926-860X(97)00266-4

[18] Lahiri, P. Sengupta, S.K. (1995). Physico-chemical properties and catalytic activities of the spinel series MnxFe$_{3-x}$O$_4$ towards peroxide decomposition. Journal of the Chemical Society, Faraday Transactions, 91(19): 3489-3494. https://doi.org/10.1039/FT9959103489

[19] Cota, H.M., Katan, T., Chin, M., Schoenweis, F.J. (1964). Decomposition of dilute hydrogen peroxide in alkaline solutions, Nature, 203:1281. https://doi.org/10.1038/2031 281a0

[20] Rajaram, R.R., Sermon, P.A. (1985). Adsorption and catalytic properties of Co$_x$Fe$_{3-x}$O$_4$ spinels. Part 1.— Preparation and characterization of precursors to ammonia-synthesis catalysts. Chem. Soc. Faraday Trans, 81(11): 2577-2591. https://doi.org/10.1039/F19858102577

[21] Harold, H.K., Mayfair, C.K. (1985). Selective oxidative dehydrogenation of butenes on ferrite catalysts, Adv. Catal., 33: 159-198. https://doi.org/10.1016/S0360-0564 (08)60260-6

[22] Trasatti, S., Lodi, G. (1981). Electrodes of conductive metallic oxides, Trasatti S. (Eds) Part B, Elsevier, Amsterdam, pp. 521-625.

[23] Iwakura, C., Nishioka, M., Tamura, H. (1982). Oxygen evolution on spinel-type ferrite film electrodes, Nippon Kagaku Kashi, 7: 1136-1140. https://doi.org/10.1246/ nikkashi.1982.1136

[24] Orehotsky, J., Huang, H., Davidson, C.R., Srinivasan S. (1979). Oxygen evolution on Ni$_x$Fe$_{3-x}$O$_4$ electrodes. Electroanal. Chem, 95(2): 233-235. https://doi.org/10.1016 /S0022-0728(79)80324-1

[25] Prasad, S., Gajbhiye, N.S. (1998). Magnetic studies of nanosized nickel ferrite particles synthesized by the citrate precursor technique. Alloys Compd, 265(1-2): 87-92. https://doi.org/10.1016/S0925-8388(97)00431-3

[26] Yang, J.M., Tsuo, W.J., Yen, F.S. (1999). Preparation of ultrafine nickel ferrite powders using mixed Ni and Fe tartrates. Solid State Chem., 145(1): 50-57. https://doi.org/10.1006/jssc.1999.8215

[27] Chen, D.H., He, X.R. (2001). Synthesis of nickel ferrite nanoparticles by sol-gel method, Materials Research Bulletin, 36(7-8): 1369-1377. https://doi.org/10.1016/S00255408(01)006 20-1

[28] Zhou, J., Ma, J., Sun, C., Xie, L., Zhao, Z., Tian, H., Wang, Y., Tao, J., Zhu, X. (2005). Low-Temperature Synthesis of $NiFe_2O_4$ by a Hydrothermal Method. Am. Ceram. Soc, 88(12): 3535-3537. https://doi.org/10.1111/j.15512916.2005.0 0629.x

[29] El Baydi, M., Poillerat, G., Rehspringer, J.L., Gautier, J.L., Koenig, J.F., Chartier, P. (1994). A sol-gel route for the preparation of Co_3O_4 catalyst for oxygen electrocatalysis in alkaline medium. Solid State Chem., 109(2): 281-288. https://doi.org/10.1006/jssc.1994.1105

[30] Martin de Vidales, J.L., Garcia Martinez, O., Vila, E., Rojas, R.M., Torralvo, M.J. (1993). Low temperature preparation of manganese cobaltite spinels [$MnxCo3−xO4$ ($0 \leqslant x \leqslant 1$)]. Materials research bulletin, 28(11): 1135-1143. https://doi.org/10.1016 /0025-5408(93)90093-S

[31] Singh, N.K., Tiwari, S.K., Anitha, K.L., Singh, R.N. (1996). Electrocatalytic properties of spinel-type $Mn_xFe_{3-x}O_4$ synthesized below 100 °C for oxygen evolution in KOH solutions. Chem. Soc. Faraday Trans, 92(13): 2397-2400. https://doi.org/10.1039/FT9969202397

[32] Li, G.H., Dai, L.Z., Lu, D.S., Peng, S.Y. (1990). Characterization of copper cobalt mixed oxide. Solid State Chemistry, 89(1): 167-173. https://doi.org/10.1016/0022 -4596(90)90308-K

[33] Singh, J.P., Singh, N.K., Singh, R.N. (1999). Electrocatalytic activity of metal-substituted Fe_3O_4 obtained at low temperature for O_2 evolution. Hydrogen Energy, 24(5): 433-439. https://doi.org/10.1016/ S0360-3199(98)00084-6

[34] Singh, R. N., Singh, J. P., Lal, B., & Singh, A. (2007). Preparation and characterization of $CuFe_{2-x}Cr_xO_4$ ($0 \leqslant x \leqslant 1.0$) nano spinels for electrocatalysis of oxygen evolution in alkaline solutions. International journal of hydrogen energy, 32(1): 11-16. https://doi.org/10.1016/j.ijhydene.2006.06.001

[35] Singh, N.K., Singh, R.N. (1999). Electrocatalytic properties of spinel type $Ni_xFe_{3-x}O_4$ synthesized at low temperature for oxygen evolution in KOH solutions. Chem., 38A: 491-495. http://hdl.handle.net/123456789/15731

[36] Singh, R.N., Singh, J.P., Singh, A. (2008). Electrocatalytic properties of new spinel-type $MMoO_4$ (M = Fe, Co and Ni) electrodes for oxygen evolution in alkaline solutions. Hydrogen Energy, 33: 4260-4264. https://doi.org/10.10 16/j.ijhydene.2008.06.008

[37] Singh, R.N., Singh, J.P., Lal, B., Thomas, M.J.K., Bera, S. (2006). New $NiFe_{2−x}Cr_xO_4$ spinel films for O_2 evolution in alkaline solutions. Electrochim Acta, 51(25): 5515-5523. https://doi.org/10.1016/j.electacta.2006.02.028

[38] Singh, R.N., Singh, J.P., Cong, N.H., Chartier, P. (2006). Effect of partial substitution of Cr on electrocatalytic properties of $MnFe_2O_4$ towards O_2-evolution in alkaline

medium. Hydrogen Energy, 31(10): 1372-1378. https://doi.org/10.1016/j.ijhydene.2005.11 .012

[39] Anindita, Singh, A., Singh, R.N. (2010). Effect of V substitution at B-site on the physicochemical and electrocatalytic properties of spinel-type $NiFe_2O_4$ towards O_2 evolution in alkaline solutions. Hydrogen Energy, 35(8): 3243-3248. https://doi.org/10.1016/j.ijhydene.2010.02. 003

[40] Yadav, R., Jhasaketan, Singh, N.K. (2015). Electrocatalytic activity of $Ni_xFe_{3-x}O_4$ ($0 \leqslant x \leqslant 1.5$) obtained by natural egg ovalbumin for alkaline water electrolysis. Electrochem. Sci., 10(11): 9297-9309. http://creativecommons.org/licenses/by/4.0/

[41] Singh, N.K., Yadav, R., Yadav, M.K. (2016). Electrocatalytic properties of novel egg-white sol-gel derived $Mn_xFe_{3-x}O_4$ ($0 \leq x \leq 1.5$) for alkaline water electrolysis. New Mat. Electrochem. Systems, 19: 209-215. https://doi.org/10.14447/jnmes.v19i4.281

[42] Yadav, R., Yadav, M.K., Singh, N.K. (2013). Electroccatalytic properties of sol-gel derived spinel $Co_xFe_{3-x}O_4$ ($0 \leqslant x \leqslant 1.5$) electrodes for oxygen evolution in alkaline solution. Electrochem. Sci., 8: 6321-6331.

[43] Singh, N.K., Yadav, R., Yadav, M.K., Fernandez, C. (2017). Effect of Co-substitution on the electrocatalytic properties of $Ni_{1.5}Fe_{1.5}O_4$ for oxygen evolution in alkaline solutions. New Mat. Electrochem. Systems, 20(3): 115-121. https://doi.org/10.14447/jnmes.v20i3.317

[44] Maensiri, S., Masingboon, C., Boonchom, B., Seraphin, S. (2007). A simple route to synthesize nickel ferrite ($NiFe_2O_4$) nanoparticles using egg white. Scripta Materialia, 56(9): 797-800. https://doi.org/10.1016/j.script amat.2006.09.033

[45] Tao, S., Gao, F., Liu, X., Sørensen, O.T. (2000), Preparation and gas-sensing properties of $CuFe_2O_4$ at reduced temperature, Materials Science and Engineering, B77: 172–176. https://doi.org/10.1016/S09215107(00)004 73-6

[46] Tiwari, S.K., Chartier, P., Singh, R.N. (1995). Preparation of perovskite-type oxides of cobalt by the malic acid aided process and their electrocatalytic surface properties in relation to oxygen evolution, J. Electrochem. Soc., 142(1): 148-153. https://doi.org/10.1149/1.2043854

[47] Okasha, N. (2004). Structural characterization and magnetic properties of $Zn_{1−x}Cu_xCr_{0.8}Fe_{1.2}O_4$; $0.1 \leq x \leq 0.9$, Mater. Chem. Phys., 84(1): 63-70. https://doi.org/10.1016/j. matchemphys.2003.10.002

[48] Gillot, B., Nivoix, V., Kester, E., Nusillard, O., Villete, C., Tailhades, P., Rousset, A. (1997). Reactivity toward oxygen and cation distribution in copper-manganese ferrite spinels fine powders. . Materials chemistry and physics, 48(2): 111-118. https://doi.org/10.1016/S0254-0584(97)80103-4

[49] Fradette, N., Marsan, B. (1998). Surface studies of $CuX Co_{3−X}O_4$ electrodes for the electrocatalysis of oxygen evolution. Electrochem, 145(7): 2320-2327. https: //doi.org/10.1149/1.1838637

[50] Singh, R.N., Pandey, J.P., Anitha, K.L. (1993). Preparation of electrodeposited thin films of nickel-iron alloys on mild steel for alkaline water electrolysis. Part I: studies on oxygen evolution. Hydrogen Energy, 18(6): 467-473. https://doi.org/10.1016/0360-3199(93)90002-R

[51] Wu, W., Guo, S., Zhang, J. (2018). Electrochemical behaviors of Cr(III) in molten LiF-NaF-KF Eutectic, Int. J. Electrochem. Sci., 13: 225-234. http://creativecommons .org/licenses/by/4.0/.

[52] Massot, L., Chamelot, P., Cassayre, L., Taxil, P. (2009). Electrochemical study of the Eu(III)/Eu(II) system in molten fluoride media. Electrochim Acta, 54(26): 6361-6366. https://doi.org/10.1016/j.electacta.2009.06.016

[53] Bard, A.J., Faulkner, L.R. (2001). Electrochemical Methods: Principles and Applications, 2nd (Ed), Wiley, New York.

[54] Singh, R.N., Tiwari, S.K., Singh, S.P., Singh, N.K., Poillerat, G., Chartier, P. (1996). Synthesis of (La, Sr)CoO3 perovskite films via a sol-gel route and their physicochemical and electrochemical surface characterization for anode application in alkaline water electrolysis. Chem. Soc. Faraday Trans., 92(14): 2593-2598. https://doi.org/10.1039/FT9969202593

[55] Al-Hoshan, M.S., Singh, J.P., Al-Mayouf, A.M., Al-Suhybani, A.A., Shaddad, M.N. (2012). Synthesis, physicochemical and electrochemical properties of nickel ferrite spinels obtained by hydrothermal method for the oxygen evolution reaction (OER). Electrochem. Sci., 7: 4959-4973.

[56] Yadav, R., Singh, N.K. (2018). Electrocatalytic activity of NixFe3-xO4 (0 ≤ x ≤ 1.5) film electrode for oxygen evolution in KOH solutions. Chem. Tech., 25(2): 189-195. http://nopr.niscair.res.in/handle/123456789/44354

[57] Gileadi, E. (1993). Electrode Kinetics, VCH Publishers Inc., New York, 151.

[58] Singh, R.N., Pandey, J.P., Singh, N.K., Lal, B., Chartier P., Koenig, J.F. (2000). Sol-gel derived spinel MxCo3−xO4 (M = Ni, Cu; 0 ≤ x ≤ 1) films and oxygen evolution. Electrochim Acta, 45(12): 1911-1919. https://doi.org/10.1016 /S0013-4686(99)00413-2

[59] Mills, A., Davis, H.L. (1992). Oxygen evolution redox catalysis using Ru-Adams, Electrochim. Acta, 37(7): 1217-1225. https://doi.org/10.1016/0013-4686(92)85059-T

[60] Kessler, T., Triaca, W.E., Arvia, A.J. (1994). Kinetics and mechanism of the oxygen evolution reaction at oxide-coated Co-Ni amorphous alloy electrodes. Appl. Electrochem., 24(4): 310-315. https://doi.org/10.1007/BF002 42058

[61] Nikolov, I., Darkaou, R., Zhecheva, E., Stoyanova, R., Dimitrov, N., Vitanov, T. (1997). Electrocatalytic activity of spinel related cobalties M$_x$Co$_{3−x}$O$_4$ (M = Li, Ni, Cu) in the oxygen evolution reaction. Electroanal. Chem., 429(1-2): 157-168. https://doi.org/10.1016/S0022-0728(96)050 13-9